Regular Article

Critical aspects of the random-field Ising model

Nikolaos G. Fytas[1,2,a], Panagiotis E. Theodorakis[3], Ioannis Georgiou[4], and Ioannis Lelidis[2]

[1] Applied Mathematics Research Centre, Coventry University, Coventry, CV1 5FB, UK
[2] Department of Physics, University of Athens, Panepistimiopolis, 15784 Zografos, Athens, Greece
[3] Department of Chemical Engineering, Imperial College London, London SW7 2AZ, UK
[4] Institute for Theoretical Physics and Center for Computational Materials Science, Vienna University of Technology, Wiedner Hauptstraße 8-10, 1040 Vienna, Austria

Abstract. We investigate the critical behavior of the three-dimensional random-field Ising model (RFIM) with a Gaussian field distribution at zero temperature. By implementing a computational approach that maps the ground-state of the RFIM to the maximum-flow optimization problem of a network, we simulate large ensembles of disorder realizations of the model for a broad range of values of the disorder strength h and system sizes $\mathcal{V} = L^3$, with $L \leq 156$. Our averaging procedure outcomes previous studies of the model, increasing the sampling of ground states by a factor of 10^3. Using well-established finite-size scaling schemes, the fourth-order's Binder cumulant, and the sample-to-sample fluctuations of various thermodynamic quantities, we provide high-accuracy estimates for the critical field h_c, as well as the critical exponents ν, β/ν, and $\bar{\gamma}/\nu$ of the correlation length, order parameter, and disconnected susceptibility, respectively. Moreover, using properly defined noise to signal ratios, we depict the variation of the self-averaging property of the model, by crossing the phase boundary into the ordered phase. Finally, we discuss the controversial issue of the specific heat based on a scaling analysis of the bond energy, providing evidence that its critical exponent $\alpha \approx 0^-$.

1 Introduction

The RFIM is one of the archetypal disordered systems [1–3], extensively studied due to its theoretical interest, as well as its close connection to experiments in hard [4,5] and soft condensed matter systems [6]. Its beauty is that the mixture of random fields and the standard Ising model creates rich physics and leaves many still unanswered problems. The Hamiltonian describing the model is

$$\mathcal{H} = -J \sum_{\langle i,j \rangle} \sigma_i \sigma_j - \sum_i h_i \sigma_i, \qquad (1)$$

where $\sigma_i = \pm 1$ are Ising spins, $J > 0$ is the nearest-neighbor's ferromagnetic interaction, and h_i are independent quenched random fields.

The existence of an ordered ferromagnetic phase for the RFIM, at low temperature and weak disorder, followed from the seminal discussion of Imry and Ma [1], when the space dimension is greater than two $(d > 2)$ [7–11]. This has provided us with a general qualitative agreement on the sketch of the phase boundary, separating the ordered ferromagnetic phase from the high-temperature paramagnetic one. The phase-diagram line separates the two

phases of the model and intersects the randomness axis at the critical value of the disorder strength h_c, as shown in Figure 1. Such qualitative sketching has been commonly used for the RFIM [12–14] and closed form quantitative expressions are also known from the early mean-field calculations [15–17]. However, it is generally true that the quantitative aspects of phase diagrams produced by mean-field treatments provide rather poor approximations.

The criteria for determining the order of the phase transition and its dependence on the field distribution have been discussed throughout the years [15–26]. In fact, different results have been proposed for different field distributions, like the existence of a tricritical point at the strong disorder regime of the system, present only in the bimodal case [15–17,20]. Currently, despite the huge efforts recorded in the literature, a clear picture of the model's critical behavior is still lacking. Although the view that the phase transition of the RFIM is nowadays considered to be of second order [27–32], the extremely small value of the exponent β continues to cast some doubts. Moreover, a rather strong debate exists with regards to the role of disorder: the available simulations are not able to settle the question of whether the critical exponents depend on the particular choice of the distribution for the random fields, analogously to the mean-field theory
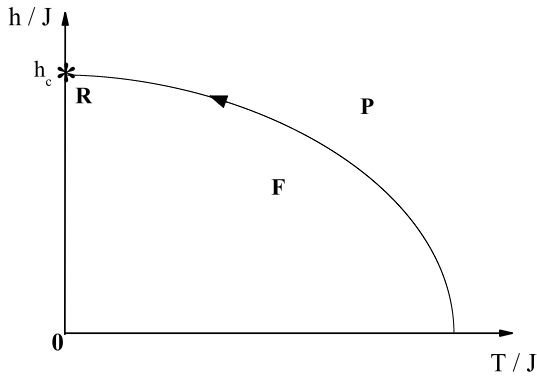
[a] e-mail: nfytas@phys.uoa.gr

Fig. 1. Schematic phase diagram and renormalization-group flow of the RFIM. The solid line separates the ordered ferromagnetic (**F**) and disordered paramagnetic (**P**) phases. The black arrow shows the flow to the random fixed-point (**R**) at $T = 0$ and $h = h_c$, marked by the asterisk.

predictions [15–17]. Thus, the whole issue of the model's critical behavior, is under intense investigation [27–48].

The scope of the present work is to shed some light towards this direction by examining several critical features of the phase diagram of the RFIM at $d = 3$. To this end, we recruit powerful numerical and finite-size scaling (FSS) techniques in order to obtain accurate numerical data through extensive simulations. On technical grounds, we implement optimization methods at zero temperature ($T = 0$) combined with a Gaussian distribution of random fields, given by the formula

$$\mathcal{P}(h_i) = \frac{1}{\sqrt{2\pi h^2}} \exp\left(-\frac{h_i^2}{2h^2}\right). \qquad (2)$$

The main advantage of the above distribution is that the ground state of the system is non-degenerate, so it is sufficient to calculate just one ground state in order to get the necessary information. Note here that, for cases of discrete distributions, like the bimodal, degeneracy complicates the numerical solution of the system at $T = 0$, since one has to sweep over all the possible ground states of the system [49–53]. On physical grounds, our attempt benefits from classical FSS techniques, and a scaling approach that involves, on one hand the fourth-order's Binder cumulant (a common measure of FSS that has been disregarded in the study of the RFIM), and on the other hand, the sample-to-sample fluctuations of the system.

In particular, sample-to-sample fluctuations and the related issue of self averaging have attracted much interest in the study of disordered systems [54]. Although it has been known for many years now that for (spin and regular) glasses there is no self-averaging in the ordered phase [55], for random ferromagnets such a behavior was first observed for the RFIM by Dayan et al. [56] and some years later for the random versions of the Ising and Ashkin-Teller models [57,58]. Ever since, the subject of breakdown of self averaging is an important aspect of several theoretical and numerical investigations of disordered spin systems [59–72]. In view of this increasing interest, we discuss here another successful alternative approach to

the criticality of the RFIM via its sample-to-sample fluctuations at $T = 0$.

The rest of the paper is organized as follows: in the next section we describe briefly the numerical approach and provide all the necessary details of our implementation. The relevant FSS analysis is presented in Section 3. In particular, we give refined estimates of the critical disorder strength h_c and the critical exponent ν using two completely independent routes: (i) the well-established FSS of the fourth-order's Binder cumulant [73]; and (ii) an approach based on the sample-to-sample fluctuations of the model. Additionally, we provide estimates for the magnetic exponent ratios β/ν and $\bar{\gamma}/\nu$, though the scaling of the order-parameter and disconnected susceptibility data at the critical field h_c. We also investigate the self-averaging properties of the model, using properly defined noise to signal ratios of the bond- and field-energy, and scanning the complete h-regime of the phase diagram well into the ordered phase of the model. Finally, we discuss the controversial issue of the specific heat of the RFIM by studying the scaling behavior of the bond energy at the proposed critical randomness h_c. We synopsize our findings in Section 4.

2 Simulation scheme

As already discussed extensively in the literature (see Ref. [74] and references therein), the RFIM captures essential features of models in statistical physics that are controlled by disorder and have frustration. Such systems show complex energy landscapes due to the presence of large barriers that separate several meta-stable states. When such models are studied using simulations mimicking the local dynamics of physical processes, it takes an extremely long time to encounter the exact ground state. However, there are cases where efficient methods for finding the ground state can be utilized and, fortunately, the RFIM is one such case. These methods escape from the typical direct physical representation of the system, in a way that extra degrees of freedom are introduced and an expanded problem is finally solved. By expanding the configuration space and choosing proper dynamics, the algorithm practically avoids the need of overcoming large barriers that exist in the original physical configuration space. An attractor state in the expended space is found in time polynomial in the size of the system and when the algorithm terminates, the relevant auxiliary fields can be projected onto a physical configuration, which is the guaranteed ground state.

The random field is a relevant perturbation at the pure fixed-point, and the random-field fixed-point is at $T = 0$ [7–10]. Hence, the critical behavior is the same everywhere along the phase boundary of Figure 1, and we can predict it simply by staying at $T = 0$ and crossing the phase boundary at $h = h_c$. This is a convenient approach, because we can determine the ground states of the system exactly using efficient optimization algorithms [27,28,32,68,69,75–80] through an existing mapping of the ground state to the maximum-flow

optimization problem [81]. A clear advantage of this approach is the ability to simulate large system sizes and disorder ensembles in rather moderate computational times. We should underline here that, even the most efficient $T > 0$ Monte Carlo schemes exhibit extremely slow dynamics in the low-temperature phase of these systems and are upper bounded by linear sizes of the order of $L_{\max} \leq 32$ [74]. Further advantages of the $T = 0$ approach are the absence of statistical errors and equilibration problems, which, on the contrary, are the two major drawbacks encountered in the $T > 0$ simulation of systems with rough free-energy landscapes [5].

In particular, the application of maximum-flow algorithms to the RFIM is nowadays well established [79]. The most efficient network flow algorithm used to solve the RFIM is the push-relabel algorithm of Tarjan and Goldberg [82]. For the interested reader, general proofs and theorems on the push-relabel algorithm can be found in standard textbooks [81]. The version of the algorithm implemented in our study involves a modification proposed by Middleton and co-workers [28,83,84] that removes the source and sink nodes, reducing memory usage and also clarifying the physical connection [83,84]. The algorithm starts by assigning an excess x_i to each lattice site i, with $x_i = h_i$. Residual capacity variables r_{ij} between neighboring sites are initially set to J. A height variable u_i is then assigned to each node via a global update step. In this global update, the value of u_i at each site in the set $\mathcal{T} = \{j | x_j < 0\}$ of negative excess sites is set to zero. Sites with $x_i \geq 0$ have u_i set to the length of the shortest path, via edges with positive capacity, from i to $\mathcal{T}$.

The ground state is found by successively rearranging the excesses x_i, via *push* operations, and updating the heights, via *relabel* operations. When no more pushes or relabels are possible, a final global update determines the ground state, so that sites which are path connected by bonds with $r_{ij} > 0$ to $\mathcal{T}$ have $\sigma_i = -1$, while those which are disconnected from $\mathcal{T}$ have $\sigma_i = 1$. A push operation moves excess from a site i to a lower height neighbor j, if possible, that is, whenever $x_i > 0$, $r_{ij} > 0$, and $u_j = u_i - 1$. In a push, the working variables are modified according to $x_i \to x_i - \delta$, $x_j \to x_j + \delta$, $r_{ij} \to r_{ij} - \delta$, and $r_{ji} \to r_{ji} + \delta$, with $\delta = \min(x_i, r_{ij})$. Push operations tend to move the positive excess towards sites in $\mathcal{T}$. When $x_i > 0$ and no push is possible, the site is relabelled, with u_i increased to $1 + \min_{\{j | r_{ij} > 0\}} u_j$. In addition, if a set of highest sites $\mathcal{U}$ become isolated, with $u_i > u_j + 1$, for all $i \in \mathcal{U}$ and all $j \notin \mathcal{U}$, the height u_i for all $i \in \mathcal{U}$ is increased to its maximum value, N, as these sites will always be isolated from the negative excess nodes. Periodic global updates are often crucial to the practical speed of the algorithm [83,84]. Following the suggestions of references [28,83,84], we have also applied global updates here every $\mathcal{V}$ relabels, a practice found to be computationally optimum [32,80,83,84].

Using this scheme we performed large-scale simulations of the RFIM for lattice sizes in the range $L \in \{L_{\min} - L_{\max}\}$, where $L_{\min} = 24$ and $L_{\max} = 156$, and disorder strengths $h \in [2.0–3.0]$ with a step $\delta h = 0.02$. Finally, for

each pair $(L; h)$ an extensive disorder averaging process has been undertaken, by sampling over $\mathcal{N}_s = 50 \times 10^3$ independent random-field realizations, much larger than in previous relevant studies of the model [28,68,69,76,77].

3 Finite-size scaling analysis

As the outcome of the push-relabel algorithm is the spin configuration of the ground state, we can calculate directly for a given sample of a lattice with linear size L some quantities of interest, as the magnetization per spin (i.e., the order parameter of the system) via

$$m = \mathcal{V}^{-1} \sum_i \sigma_i. \tag{3}$$

Taking now the average over different independent disorder configurations we may define the sample-averaged order parameter $M = [|m|]$ (see main panel of Fig. 7), and also the disconnected susceptibility $\chi_{\mathrm{dis}} = \mathcal{V}[m^2]$. Subsequently, the fourth-order's Binder cumulant is given by [85]

$$g(h, L) = \frac{1}{2} \left\{ 3 - \frac{[m^4]}{[m^2]^2} \right\}. \tag{4}$$

Another physical parameter of interest is the bond energy per spin that corresponds to the first term of the Hamiltonian (1), i.e. $e_J = -\mathcal{V}^{-1} \sum_{\langle i,j \rangle} \sigma_i \sigma_j$, and its disorder average, defined hereafter as $E_J = [e_J]$. Similarly, the disorder-averaged random-field energy per spin (second term in Hamiltonian (1)) is defined as E_{rf}.

3.1 Fourth-order's Binder cumulant

We start the presentation of our analysis with the crossing and scaling properties of the fourth-order's Binder cumulant. In Figure 2, we plot the fourth-order's Binder cumulant (4) as a function of the random-field strength h for the complete range of the simulated lattice sizes, as shown by the different colors. Respectively, in the corresponding inset we show an enlargement of the curves in the field area around the value $h \approx 2.27$, where they are expected to cross [28]. Indeed, as can be seen from the enlargement, the curves cross in the area $2.265 \leq h \leq 2.28$, indicating that we can apply the well-established FSS procedure, using the infinite limit-size extrapolation of the crossings of lattice-size pairs $(L_1, L_2) = (L, 2L)$ in order to obtain an estimate of the critical field. Figure 3 illustrates the scaling behavior of these crossings as a function of the inverse (new) linear size L' (see definition below). We show five data points h^*_{cross} and their relevant errors, obtained after performing spline interpolations to the cumulant curves, for the following pairs of lattices: $(L_1, L_2) = (24, 48)$, $(32, 64)$, $(48, 96)$, $(64, 128)$, and $(78, 156)$. The notation L' in the horizontal axis refers to the value $L' = (L_1 + L_2)/2$. The solid line is a linear fitting extrapolation to $L' \to \infty$ with a good-quality value of $\chi^2/\mathrm{dof} = 0.8$ (where dof denotes the number of degrees of freedom), which gives the
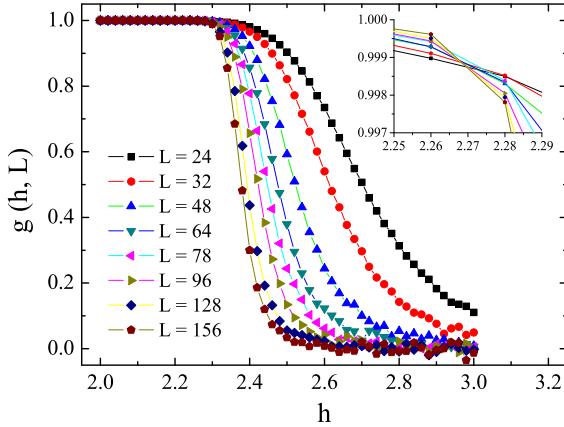
Fig. 2. Fourth-order's Binder cumulant (4) as a function of the random-field strength h for linear sizes $L = 24$–156. The inset is an enlargement of the critical area that shows a clear crossing of the curves around the expected value $h_c \approx 2.27$. The lines are simple guides to the eye.
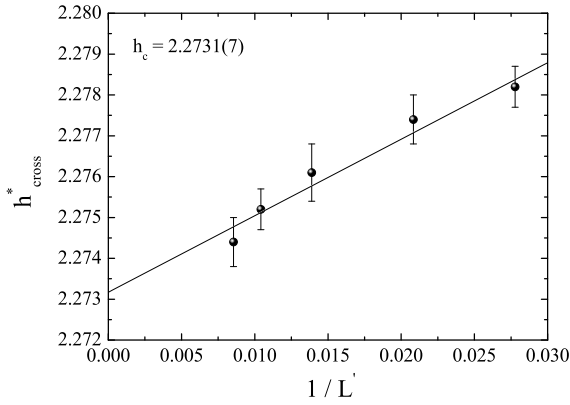

Fig. 3. Estimation of the critical disorder strength h_c via the infinite limit-size extrapolation of the crossings of the fourth-order's Binder cumulant.

estimate $h_c = 2.2731(7)$ for the critical field of the $d = 3$ Gaussian RFIM. This value is a refined estimate of previous calculations and is in good agreement with very good estimates in the current literature [28,68,69,76].

At this point we provide a further verification of the above h_c-estimate, together with an independent calculation of the critical exponent ν of the correlation length, using again the scaling behavior of the fourth-order's Binder cumulant (4). The standard theory of FSS indicates that the Binder cumulant scales as

$$g(h, L) = \tilde{g}\left[(h - h_c)L^{1/\nu}\right], \quad (5)$$

where the equality is a result of the dimensionless definition of the Binder cumulant. Using a properly chosen h-axis re-scaling function, the Binder cumulant for all system sizes belonging to the same dimension collapses onto one single master curve. Figure 4 illustrates, using the reduced scaling variable $(h - h_c)L^{1/\nu}$, the optimum data collapse of $g(h, L)$ for different system sizes in the range $L = 48$–156, obtained for parameters $h_c = 2.2725$ and
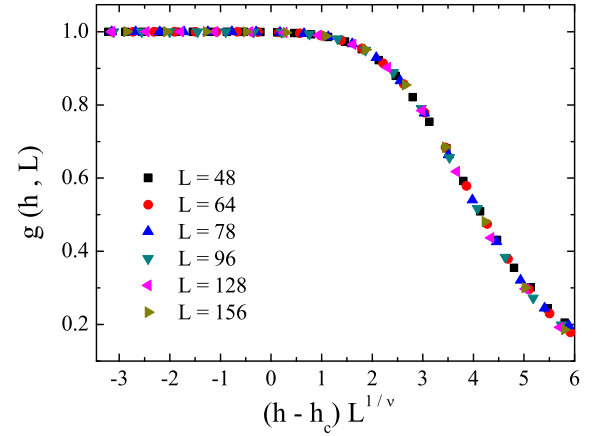

Fig. 4. Data collapse of the Binder cumulant for different systems withe linear sizes in the range $L = 48$–156. The optimum collapse is obtained for $h_c = 2.2725$ and $\nu = 1.375$.

$\nu = 1.375$. The resulting value of the critical field h_c compares well to the estimate 2.2731(7) of Figure 3 obtained via the infinite limit-size extrapolation of the crossings of the same quantity, and the value $\nu = 1.375$ is in excellent agreement with the widely accepted estimate 1.37(9) [28].

3.2 Sample-to-sample fluctuations

As already discussed in the introduction, the role of sample-to-sample fluctuations in random spin models has recently attracted much interest, due to its close connection with important physical phenomena taking place in the boundary among the phases of the system. In this section we present another successful application of the fluctuations of the RFIM, obtaining at the same time accurate results for its critical point h_c and the correlation-length's exponent ν.

At this point, let us start the presentation of our FSS approach with Figure 5, where we plot the sample-to-sample fluctuations over disorder of two quantities, namely the random-field energy per spin E_{rf} (panel (a)) and the disconnected susceptibility χ_{dis} (panel (b)). Both fluctuations are plotted as a function of the disorder strength h for the complete lattice size-range $L = 24$–156. It is clear that, for every lattice size L, these fluctuations appear to have a maximum value at a certain value of h, denoted hereafter as h_L^*, that may be considered in the following as a suitable pseudo-critical disorder strength. By fitting the data points around the maximum first to a Gaussian, and subsequently to a fourth-order polynomial function, we have extracted the values of the peak locations (h_L^*) by taking the mean value via the two fitting functions, as well as the corresponding errors. Using now these values for h_L^* we consider in Figure 6 a simultaneous power-law fitting attempt of the form

$$h_L^* = h_c + bL^{-1/\nu}. \quad (6)$$

The quality of the fit is fair enough, with a value of χ^2/dof of the order of 0.4, and produces the estimates

Table 1. Summary of estimates for the critical field h_c and typical critical exponents of the $d = 3$ Gaussian RFIM, as given in the present and in some of the most comprehensive $T > 0$ Monte Carlo (MC) and $T = 0$ ground-state (GS) simulation studies. The maximum lattice size (L_{max}) considered and the number of disorder samples $\mathcal{N}_s$, in units of 10^2, that corresponds to this L_{max}, are also given for statistical comparison.

Reference	Method	L_{max}	$\mathcal{N}_s \times 10^2$	h_c	ν	β/ν	$\bar{\gamma}/\nu$	α
[14]	MC	32	1	2.23(2)	1.02(6)	0.06(7)	2.84(7)	
[27]	GS	80	2	2.29(4)	1.19(8)	0.017(9)	2.94(5)	
[28]	GS	256	20	2.270(4)	1.37(9)	0.011(3)		−0.01(9)
[33,34]	MC	16	10		1.1(2)	0.00(5)	2.97(5)	−0.5(2)
[68,69]	GS	96	20	2.282(2)	1.25(2)			−0.05(2)
[76]	GS	96	38	2.28(1)	1.32(7)			−0.63(7)
[77]	GS	60	1	2.29(2)	1.1(1)			0.1(1)
This work	GS	156	500	2.272(3)	1.38(2)	0.013(1)	2.974(2)	−0.09(5)

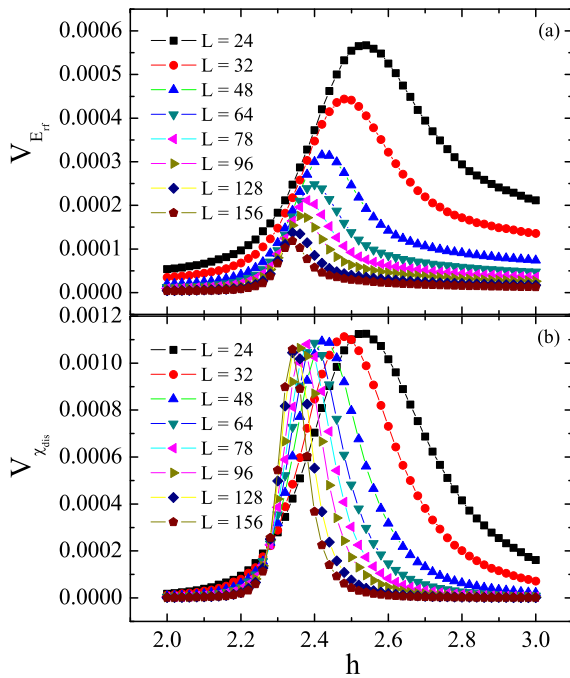**Fig. 5.** Sample-to-sample fluctuations of the field energy $V_{E_{rf}}$ (a) and disconnected susceptibility $V_{\chi_{dis}}$ (b) of the Gaussian RFIM as a function of the disorder strength for various lattice sizes in the range $L = 24$–156. Lines are simple guides to the eye.

Fig. 6. Simultaneous fitting (6) of the pseudo-critical disorder strengths h_L^*, obtained from the peak positions of the fluctuations shown in Figure 5. The shared parameters of the two data sets of the fit are the critical disorder strength h_c and the correlation length's exponent ν.

$h_c = 2.270(3)$ and $\nu = 1.38(2)$ for the critical disorder strength and the correlation length's exponent. These values corroborate the previous estimates of Section 3.1 and, furthermore, compare very well to the most accurate estimates of the literature (see Tab. 1 in Sect. 4). The final value we quote for the critical field is taken as an average among the two estimations to be $h_c = 2.272(3)$.

We note here that our suggestion of choosing these newly defined pseudo-critical disorder strengths h_L^* as a proper measure for performing FSS, closely follows the analogous considerations of Hartmann and Young [76] and Dukovski and Machta [77], also for the Gaussian RFIM, and of reference [80] for the RFIM with a trimodal distribution of random fields. The first authors [76] considered
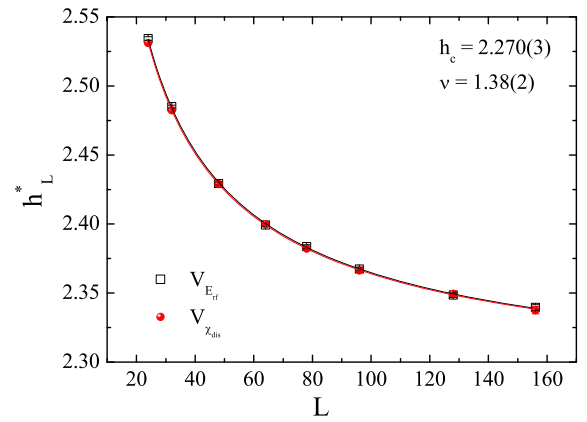
pseudo-critical disorder strengths at the values of h at which a specific-heat-like quantity obtained by numerically differentiating the bond energy with respect to h attains its maximum. On the other hand, the authors of reference [77] identified the pseudo-critical points as those in the H-h plane (with H a uniform external field), where three degenerate ground states of the system show the largest discontinuities in the magnetization. Finally, in reference [80], the location of the maximum of the order-parameter's fluctuations was used in order to probe the critical properties of the system. It appears that this method of extracting pseudo-critical points from the maxima of some properly defined thermodynamic quantity is capable of producing very accurate estimates for both the critical disorder strength and also the correlation length's exponent, assuming that its behavior follows the observed shift behavior of our pseudo-critical disorder strengths h_L^*.

The practice followed in the current paper, employing the FSS behavior of the peaks of the sample-to-sample fluctuations of several quantities of physical origin, was inspired by the intriguing analysis of Efrat and Schwartz [72]. These authors, studying also the $d = 3$
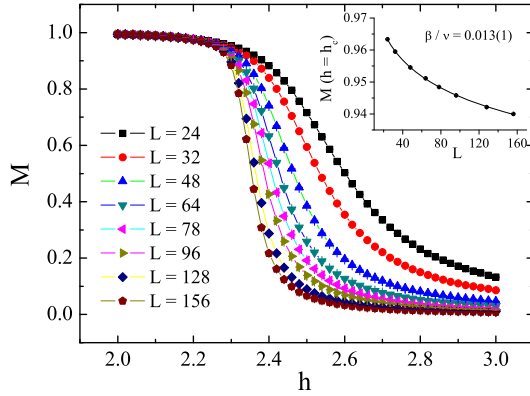
Fig. 7. Order parameter M as a function of the random-field strength h for all system sizes studied. Lines are simple guides to the eye. The inset illustrates the FSS behavior of the critical data.
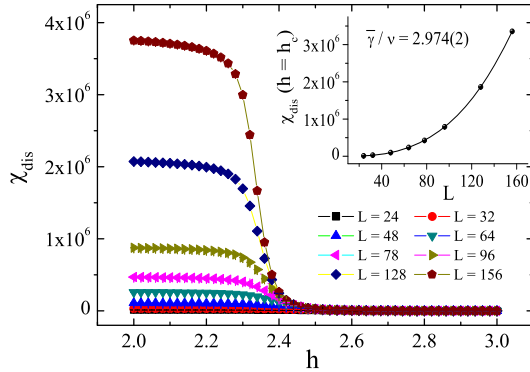

Fig. 8. The same as in Figure 7, but for the disconnected susceptibility χ_{dis}.

RFIM, showed that the behavior of the sample-to-sample fluctuations in a disordered system may be turned into a useful tool that can provide an independent measure to distinguish between the ordered and disordered phases of the system. The analysis of Figures 5 and 6 above verifies their prediction, and the accuracy in the estimation of relevant phase diagram features, like the critical field h_c and the critical exponent ν, consist a clear test in favor of the overall scheme.

3.3 Magnetic exponent ratios

The goal in this third part of our analysis is the extraction of accurate estimates for the magnetic exponent ratios β/ν and $\bar{\gamma}/\nu$, via the scaling of the order parameter M and disconnected susceptibility χ_{dis}, respectively. As we have at hand a high-accuracy estimate of the critical field, $h = 2.272$, we follow the standard FSS approach, i.e., the investigation of the asymptotic approach of the critical values of M and χ_{dis} to $L \to \infty$. The general form of the order parameter M and disconnected susceptibility χ_{dis} as a function of the random-field strength h is shown in the main panels of Figures 7 and 8, respectively, for the complete range of lattice sizes studied. The fitting extrapolations of their critical values (at $h = h_c$) are shown in the

corresponding insets, using the typical power-law forms $M(h = h_c) \sim L^{-\beta/\nu}$ and $\chi_{\mathrm{dis}}(h = h_c) \sim L^{\bar{\gamma}/\nu}$. The resulting estimates of the magnetic exponent ratios, given also in the figures, are $\beta/\nu = 0.013(1)$ and $\bar{\gamma}/\nu = 2.974(2)$. This latter estimate suggests, through the relation $\bar{\eta} = 4 - \bar{\gamma}/\nu$, the value $\bar{\eta} = 1.026(2)$ for the critical exponent that describes the power-law decay of the disconnected correlation function of the RFIM. Overall, both values of β/ν and $\bar{\gamma}/\nu$ are refinements of previously obtained estimates (see Tab. 1 for details and a direct comparison among previous works), and moreover, the value of $\bar{\eta}$ is in agreement with the value $\bar{\eta} = 1$, that can be predicted from elementary considerations in the ordered phase [56] and the results of high-temperature series expansions of the RFIM [25,26].

3.4 Self-averaging properties

Following the discussion of Section 3.2, our numerical studies of disordered systems are carried out near their critical points using finite samples; each sample is a particular random realization of the quenched disorder. A measurement of a thermodynamic property, say Z, yields a different value for every sample. In an ensemble of disordered samples of linear size L the values of Z are distributed according to a probability distribution. The behavior of this distribution is directly related to the issue of self-averaging. In particular, by studying the behavior of the width of this distribution, one may address qualitatively the issue of self-averaging, as has already been stressed by previous authors [57,58,61]. In general, we characterize the distribution by its average $[Z]$ and also by the relative variance

$$R_Z = \frac{V_Z}{[Z]^2} = \frac{[Z^2] - [Z]^2}{[Z]^2}, \tag{7}$$

that we employ here to investigate the self-averaging properties of the RFIM.

In particular, we study the behavior of the ratio R_Z, in the framework of the two main quantities in this paper, the random-field energy E_{rf} and the bond energy E_J of the model. In our $T = 0$ formalism, we define an h-dependent formula of R_Z, shown in the main panel ($Z = E_{\mathrm{rf}}$) and inset ($Z = E_J$) of Figure 9 for three lattice sizes, $L = 64$, 78, and $L = 128$, as indicated by the different colors. Our intention is to identify the variation of this ratio, as we approach the ordered phase. Although the bond energy exhibits a maximum in the vicinity of the phase boundary of each system size (note that the h-value of the maximum is close to the respective value shown in Fig. 5), as we enter the ordered phase ($h \leq h_L^*$) the ratio R_{E_J} goes smoothly to zero, indicating a restoration of self-averaging (see inset of Fig. 9). On the other hand, the violation of self-averaging for the random-field energy, as given by the behavior of the ratio $R_{E_{\mathrm{rf}}}$ (main panel of Fig. 9), becomes maximal in the ordered phase, indicating strong sample-to-sample fluctuations and non self-averaging behavior, in agreement with previous studies [56,72]. Let us comment here that, possible breakdown of self-averaging may be traced back to situations where the correlation length ξ becomes of
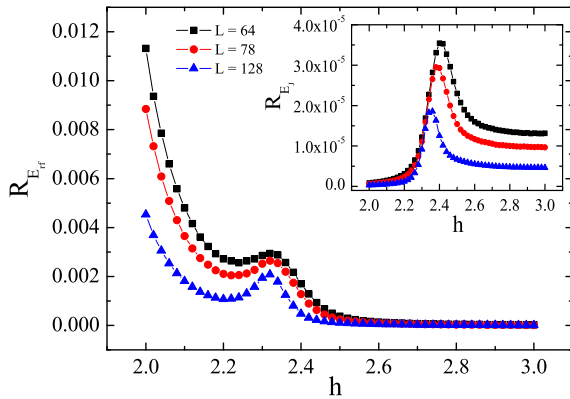
Fig. 9. Disorder-strength variation of the ratio (7) for $E_{\rm rf}$ (main panel) and $E_{\rm J}$ (inset) and three lattice sizes, as indicated by the different colors in both panels.
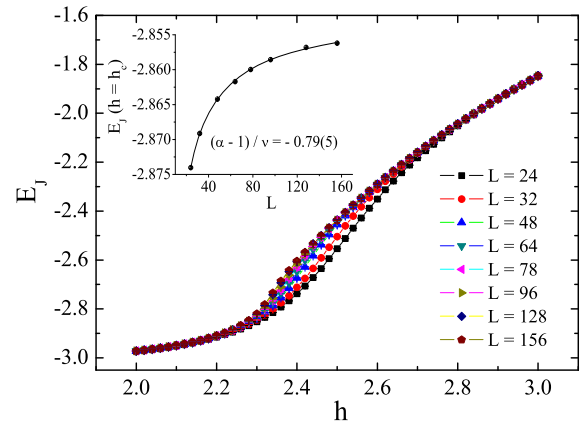

Fig. 10. Disorder-averaged bond energy per spin as a function of the random-field strength h for all system sizes studied. Lines are simple guides to the eye. The inset illustrates the FSS behavior of $E_{\rm J}$ at the suggested critical value $h_{\rm c} = 2.272$.

the order of the linear size of the system. The usual state of affairs is that the correlation length diverges just on the boundary between the ordered and disordered phase and consequently any break down of self-averaging may be observed only in the vicinity of the boundary [58,61,72]. However, as Dayan et al. [56] showed, the situation in the RFIM is quite different: the correlation length is of order of the linear size of the system everywhere in the ordered phase and not just at the boundary of the phase, indicating possible violations of self-averaging also in the ordered phase, as in the main panel of Figure 9.

3.5 Scaling aspects of the bond energy

The last part of our FSS analysis concerns the controversial issue of the specific heat of the RFIM. The specific heat of the RFIM can be experimentally measured [86,87] and is, for sure, of great theoretical importance. Yet, it is well known that it is one of the most intricate thermodynamic quantities to deal with in numerical simulations, even when it comes to pure systems. For the RFIM, Monte Carlo methods at $T > 0$ have been used to estimate the value of its critical exponent α, but were restricted to rather small systems sizes and have also revealed many serious problems, i.e., severe violations of self averaging [64,67]. A better picture emerged throughout the years from $T = 0$ computations, proposing estimates of $\alpha \approx 0$. However, even by using the same numerical techniques, but different scaling approaches, some inconsistencies have been recorded in the literature. The most prominent was that of reference [76], where a strongly negative value of the critical exponent α was estimated. On the other hand, experiments on random field and diluted antiferromagnetic systems suggest a clear logarithmic divergence of the specific heat [86,87].

In general, one expects that the finite-temperature definition of the specific heat C can be extended to $T = 0$, with the second derivative of $\langle E \rangle$ with respect to temperature being replaced by the second derivative of the ground-state energy density $E_{\rm gs}$ with respect to the random field h [28,76]. The first derivative $\partial E_{\rm gs}/\partial J$

is the bond energy $E_{\rm J}$, already defined above (see main panel of Fig. 10). The general FSS form assumed is that the singular part of the specific heat $C_{\rm s}$ behaves as $C_{\rm s} \sim L^{\alpha/\nu}\tilde{C}\left[(h - h_{\rm c})L^{1/\nu}\right]$. Thus, one may estimate α by studying the behavior of $E_{\rm J}$ at $h = h_{\rm c}$ [28]. The computation from the behavior of $E_{\rm J}$ is based on integrating the above scaling equation up to $h_{\rm c}$, which gives a dependence

$$E_{\rm J}(h = h_{\rm c}) = c_1 + c_2 L^{(\alpha-1)/\nu}, \qquad (8)$$

with c_i constants. Alternatively, following the prescription of [76], one may calculate the second derivative by finite differences of $E_{\rm J}(h)$ for values of h near $h_{\rm c}$ and determine α by fitting to the maximum of the peaks in $C_{\rm s}$, which occur at $h_{\rm L}^* - h_{\rm c} \approx L^{-1/\nu}$. However, as already noted in [28], this latter approach may be more strongly affected by finite-size corrections, since the peaks in $C_{\rm s}$ found by numerical differentiation are somewhat above $h_{\rm c}$, and furthermore it is computationally more demanding, since one must have the values of $E_{\rm J}$ in a wide and very dense range of h-values.

In the present case, where the critical value $h_{\rm c}$ is known with good accuracy, the first approach seems to be more suitable to follow. The numerical data of the critical bond energy and the relevant FSS analysis are presented in the inset of Figure 10. The solid line is a power-law fittings of the form (8) and the estimate for the exponent ratio $(\alpha - 1)/\nu$ is $-0.79(5)$, as also given in the figure. Using now our estimate $\nu = 1.38(2)$, we calculate the critical exponent α of the specific heat, resulting in an estimate $\alpha = -0.09(5)$, which is fairly compatible to the experimental scenario of a logarithmic divergence ($\alpha = 0$) [86,87]. Finally, from the modified hyper-scaling relation [9] $\theta = d - 1/\nu + (\alpha-1)/\nu$, and the above estimates of $(\alpha-1)/\nu = -0.79(5)$ and the value $\nu = 1.38(2)$, we deduce an estimate for the exponent $\theta = 1.49(3)$, in good agreement to the most accurate estimates in the modern literature, i.e., the values 1.49(3) for the Gaussian RFIM [28] and 1.469(20) for the experimental analogue of the RFIM, that is the diluted antifferomagnet in a field [30].

4 Synopsis

A summary of h_c estimates, as well as of some of the main critical exponents of the RFIM given in the present, but also in the most comprehensive numerical studies of the model, can be found in Table 1. Although, in principle, by doing some "tricky" modifications on the push-relabel algorithm one may reach sizes of the order of $L = 256$ [28], here, we decided to follow the safe route of upper bounding the simulations to $L_{max} = 156$, which is in any case larger than all other previous studies of the RFIM (see Tab. 1), but dedicate our resources to secure sampling over large ensembles of random-field realizations. We should note here that, our disorder-averaging procedure has increased the number of ground states by a factor of 10^3, thus eliminating possible obscured effects stemming from deficient disorder averaging and self-averaging violations. A careful examination of the data of Table 1 indicates that our scheme enabled us to present higher-quality estimates for several features of the phase diagram of the RFIM, i.e., the critical field h_c and the critical exponents ν, β/ν, and $\bar{\gamma}/\nu$ of the correlation length, order parameter, and disconnected susceptibility, respectively. We believe that these safe estimates will be useful for further theoretical and numerical studies of the model, not only at zero, but also at positive temperatures.

On physical grounds, we have implemented a FSS approach based on the fourth-order's Binder cumulant and the sample-to-sample fluctuations of the model, not considered explicitly in previous relevant investigations of the RFIM. The outcome of this analysis indicated that the fluctuations of the system may be used as an alternative successful approach to criticality, paving the way to even more sophisticated studies of disordered systems under this perspective. Particular interest has been paid to the self-averaging properties of the model, by presenting numerical evidence in favor of the early prediction regarding possible violations of self-averaging in the ordered phase of the RFIM. Furthermore, the controversial issue of the specific heat of the model has been addressed, via the scaling of the bond energy at the estimated critical field and accurate values for the critical exponent α of the specific heat and the violation of hyper-scaling exponent θ have been proposed, compatible with the experimental scenario and in good agreement with the current literature.

References

1. Y. Imry, S.-K. Ma, Phys. Rev. Lett. **35**, 1399 (1975)
2. A. Aharony, Y. Imry, S.-K. Ma, Phys. Rev. Lett. **37**, 1364 (1976)
3. G. Parisi, N. Sourlas, Phys. Rev. Lett. **43**, 744 (1979)
4. D.P. Belanger, A.P. Young, J. Magn. Magn. Mater. **100**, 272 (1991)
5. H. Rieger, in *Annual Reviews of Computational Physics II*, edited by D. Stauffer (World Scientific, Singapore 1995), pp. 295–341
6. R.L.C. Vink, K. Binder, H. Löwen, Phys. Rev. Lett. **97**, 230603 (2006)
7. J. Villain, Phys. Rev. Lett. **52**, 1543 (1984)
8. A.J. Bray, M.A. Moore, J. Phys.: Condens. Matter **18**, L927 (1985)
9. D.S Fisher, Phys. Rev. Lett. **56**, 416 (1986)
10. A.N. Berker, S.R. McKay, Phys. Rev. B **33**, 4712 (1986)
11. J. Bricmont, A. Kupiainen, Phys. Rev. Lett. **59**, 1829 (1987)
12. M.E.J. Newman, B.W. Roberts, G.T. Barkema, J.P. Sethna, Phys. Rev. B **48**, 16533 (1993)
13. J. Machta, M.E.J. Newman, L.B. Chayes, Phys. Rev. E **62**, 8782 (2000)
14. M.E.J. Newman, G.T. Barkema, Phys. Rev. E **53**, 393 (1996)
15. A. Aharony, Phys. Rev. B **18**, 3318 (1978)
16. A. Aharony, Phys. Rev. B **18**, 3328 (1978)
17. D. Andelman, Phys. Rev. B **27**, 3079 (1983)
18. S. Galam, J.L. Birman, Phys. Rev. B **28**, 5322 (1983)
19. V.K. Saxena, Phys. Rev. B **30**, 4034 (1984)
20. A. Houghton, A. Khurana, F.J. Seco, Phys. Rev. Lett. **55**, 856 (1985)
21. D.C. Mattis, Phys. Rev. Lett. **55**, 3009 (1985)
22. M. Kaufman, P.E. Klunzinger, A. Khurana, Phys. Rev. B **34**, 4766 (1986)
23. R.M. Sebastianes, V.K. Saxena, Phys. Rev. B **35**, 2058 (1987)
24. A.S. de Arruda, W. Figueiredo, R.M. Sebastianes, V.K. Saxena, Phys. Rev. B **39**, 4409 (1989)
25. M. Gofman, J. Adler, A. Aharony, A.B. Harris, M. Schwartz, Phys. Rev. Lett. **71**, 1569 (1993)
26. M. Gofman, J. Adler, A. Aharony, A.B. Harris, M. Schwartz, Phys. Rev. B **53**, 6362 (1996)
27. A.K. Hartmann, U. Nowak, Eur. Phys. J. B **7**, 105 (1999)
28. A.A. Middleton, D.S. Fisher, Phys. Rev. B **65**, 134411 (2002)
29. R.L.C. Vink, T. Fischer, K. Binder, Phys. Rev. E **82**, 051134 (2010)
30. L.A. Fernández, V. Martín-Mayor, D. Yllanes, Phys. Rev. B **84**, 100408(R) (2011)
31. N.G. Fytas, A. Malakis, K. Eftaxias, J. Stat. Mech. **2008**, P03015 (2008)
32. P.E. Theodorakis, I. Georgiou, N.G. Fytas, Phys. Rev. E **87**, 032119 (2013)
33. H. Rieger, A.P. Young, J. Phys. A **26**, 5279 (1993)
34. H. Rieger, Phys. Rev. B **52**, 6659 (1995)
35. A. Falicov, A.N. Berker, S.R. McKay, Phys. Rev. B **51**, 8266 (1995)
36. M.R. Swift, A.J. Bray, A. Martian, M. Cieplak, J.R. Banavar, Europhys. Lett. **38**, 273 (1997)
37. J.-C. Anglés d Auriac, N. Sourlas, Europhys. Lett. **39**, 473 (1997)
38. N. Sourlas, Comput. Phys. Commun. **121**, 183 (1999)
39. U. Nowak, K.D. Usadel, J. Esser, Physica A **250**, 1 (1998)
40. P.M. Duxbury, J.H. Meinke, Phys. Rev. E **64**, 036112 (2001)
41. L. Hernández, H. Ceva, Physica A **387**, 2793 (2008)
42. N. Crokidakis, F.D. Nobre, J. Phys.: Condens. Matter **20**, 145211 (2008)
43. O.R. Salmon, N. Crokidakis, F.D. Nobre, J. Phys.: Condens. Matter **21**, 056005 (2009)
44. I.A. Hadjiagapiou, Physica A **390**, 2229 (2011)
45. I.A. Hadjiagapiou, Physica A **390**, 3204 (2011)

46. I.A. Hadjiagapiou, Physica A **391**, 3541 (2012)
47. Ü. Akinci, Y. Yüksel, H. Polat, Phys. Rev. E **83**, 061103 (2011)
48. M. Tissier, G. Tarjus, Phys. Rev. Lett. **107**, 041601 (2011)
49. A.K. Hartmann, K.D. Usadel, Physica A **214**, 141 (1995)
50. A.K. Hartmann, Physica A **248**, 1 (1998)
51. S. Bastea, P.M. Duxbury, Phys. Rev. E **58**, 4261 (1998)
52. S. Bastea, Phys. Rev. E **58**, 7978 (1998)
53. S. Bastea, P.M. Duxbury, Phys. Rev. E **60**, 4941 (1999)
54. R. Brout, Phys. Rev. **115**, 824 (1959)
55. K. Binder, A.P. Young, Rev. Mod. Phys. **58**, 837 (1986)
56. I. Dayan, M. Schwartz, A.P. Young, J. Phys.: Condens. Matter **26**, 3093 (1993)
57. S. Wiseman, E. Domany, Phys. Rev. E **52**, 3469 (1995)
58. A. Aharony, A.B. Harris, Phys. Rev. Lett. **77**, 3700 (1996)
59. K. Eichhorn, K. Binder, J. Phys.: Condens. Matter **8**, 5209 (1996)
60. F. Pázmándi, R. Scalettar, G.T. Zimányi, Phys. Rev. Lett. **79**, 5130 (1997)
61. S. Wiseman, E. Domany, Phys. Rev. Lett. **81**, 22 (1998)
62. H.G. Ballesteros, L.A. Fernández, V. Martín-Mayor, A. Muñoz Sudupe, G. Parisi, J.J. Ruiz-Lorenzo, Phys. Rev. B **58**, 2740 (1998)
63. Y. Tomita, Y. Okabe, Phys. Rev. E **64**, 036114 (2001)
64. G. Parisi, N. Sourlas, Phys. Rev. Lett. **89**, 257204 (2002)
65. P.E. Berche, C. Chatelain, B. Berche, W. Janke, Eur. Phys. J. B **38**, 463 (2004)
66. C. Monthus, T. Garel, Eur. Phys. J. B **48**, 393 (2005)
67. A. Malakis, N.G. Fytas, Phys. Rev. E **73**, 016109 (2006)
68. Y. Wu, J. Machta, Phys. Rev. Lett. **95**, 137208 (2005)
69. Y. Wu, J. Machta, Phys. Rev. B **74**, 064418 (2006)
70. A. Gordillo-Guerrero, J.J. Ruiz-Lorenzo, J. Stat. Mech. **2007**, P0601 (2007)
71. N.G. Fytas, A. Malakis, Phys. Rev. E **81**, 041109 (2010)
72. A. Efrat, M. Schwartz, `arXiv:cond-mat/0608435` (2006)
73. D.P. Landau, K. Binder, *A Guide to Monte Carlo Simulations in Statistical Physics* (Cambridge University Press, 2000)
74. A.K. Hartmann, H. Rieger, *Optimization Algorithms in Physics* (Wiley-VCH, Berlin, 2004)
75. A.T. Ogielski, Phys. Rev. Lett. **57**, 1251 (1986)
76. A.K. Hartmann, A.P. Young, Phys. Rev. B **64**, 214419 (2001)
77. I. Dukovski, J. Machta, Phys. Rev. B **67**, 014413 (2003)
78. E.T. Seppälä, M.J. Alava, Phys. Rev. E **63**, 066109 (2001)
79. M.J. Alava, P.M. Duxbury, C.F. Moukarzel, H. Rieger, in *Phase Transitions and Critical Phenomena*, edited by C. Domb, J.L. Lebowitz (Academic Press, San Diego, 2001), Vol. 18
80. N.G. Fytas, P.E. Theodorakis, I. Georgiou, Eur. Phys. J. B **85**, 349 (2012)
81. C.H. Papadimitriou, *Computational Complexity*, (Addison-Wesley, Reading, MA, 1994)
82. A.V. Goldberg, R.E. Tarjan, J. Assoc. Comput. Mach. **35**, 921 (1988)
83. A.A. Middleton, Phys. Rev. Lett. **88**, 017202 (2002)
84. J.H. Meinke, A.A. Middleton, `arXiv:cond-mat/0502471` (2005)
85. K. Binder, Z. Phys. **43**, 119 (1981)
86. D.P. Belanger, A.R. King, V. Jaccarino, J.L. Cardy, Phys. Rev. B **28**, 2522 (1983)
87. D.P. Belanger, Z. Slanič, J. Magn. Magn. Mater. **186**, 65 (1998)